

Article

Changes in Thornthwaite Moisture Index and Reactive Soil Movements under Current and Future Climate Scenarios—A Case Study

Md Rajibul Karim , Md Mizanur Rahman , Khoi Nguyen, Donald Cameron, Asif Iqbal and Isaac Ahenkorah 

UniSA STEM, University of South Australia, Mawson Lakes Campus, Adelaide, SA 5095, Australia; mizanur.rahman@unisa.edu.au (M.M.R.); khoi.nguyen@unisa.edu.au (K.N.); Donald.Cameron@unisa.edu.au (D.C.); asif.iqbal@unisa.edu.au (A.I.); isaac.ahenkorah@mymail.unisa.edu.au (I.A.)

* Correspondence: rajibul.karim@unisa.edu.au

Abstract: Expansive soils go through significant volume changes due to seasonal moisture variations resulting in ground movements. The ground movement related problems are likely to worsen in the future due to climate change. It is important to understand and incorporate likely future changes in design to ensure the resilience of structures built on such soils. However, there has been a limited amount of work quantifying the effect of climate change on expansive soils movement and related behaviour of structures. The Thornthwaite Moisture Index (TMI) is one of the commonly used climate classifiers in quantifying the effect of atmospheric boundary on soil behaviour. Using the long-term weather data and predicted future changes under different emission scenarios, a series of TMI maps are developed for South Australia. Potential changes in ground movement are then estimated for a selected area using a simplified methodology where the effect of future climate is captured through changes in TMI. Results indicate that South Australia is likely to face a significant reduction in TMI under all emission scenarios considered in this study. The changes in TMI will lead to a considerable increase in potential ground movement which will influence the behaviour of structures built on them and in some areas may lead to premature failure if not considered in the design.

Keywords: expansive soils; ground movement; suction depth; climate change; Thornthwaite Moisture Index (TMI)



Citation: Karim, M.R.; Rahman, M.M.; Nguyen, K.; Cameron, D.; Iqbal, A.; Ahenkorah, I. Changes in Thornthwaite Moisture Index and Reactive Soil Movements under Current and Future Climate Scenarios—A Case Study. *Energies* **2021**, *14*, 6760. <https://doi.org/10.3390/en14206760>

Academic Editors: Gye-Chun Cho and Ilhan Chang

Received: 25 August 2021

Accepted: 13 October 2021

Published: 17 October 2021

Publisher's Note: MDPI stays neutral with regard to jurisdictional claims in published maps and institutional affiliations.



Copyright: © 2021 by the authors. Licensee MDPI, Basel, Switzerland. This article is an open access article distributed under the terms and conditions of the Creative Commons Attribution (CC BY) license (<https://creativecommons.org/licenses/by/4.0/>).

1. Introduction

South Australia is the driest state on the driest inhabited continent in the world. The climate here has been going through quantifiable changes since the 1960s. Similar to other parts of the world, climate change here is likely to have a significant impact on the ecosystem, agriculture, and the built environment [1]. Climate change has already been attributed to reduced rainfall and increased temperatures in South-Eastern Australia [2–4]. Cai and Cowan [2] indicated climate change is responsible for a 20% reduction in rainfall during winter since the 1960s and with the possibility of increased greenhouse gases resulting in even greater rates of rainfall reduction in the future [5]. A decrease in cool seasonal rainfall across many regions of South Australia, more intense but shorter duration heavy rainfall across Australia, and increased temperatures are going to be the features of Australian climate [1,6,7].

Climate change is already having an impact on the behaviour of geotechnical structures in many different countries [8–16]. Depending on the type of structure, local soil type, local climate and expected future changes, the impact can be different in different scenarios. Many contemporary construction or ground improvement methods use temperature and moisture-sensitive materials [17–20] and these changes need to be carefully considered to avoid unexpected losses in efficiencies of these techniques.

Climate change and its influence on soil behaviour have been an active area of research over the past two decades. However, the majority of the work has been focused on understanding the interactions involved in the soil–atmospheric boundary investigating soil–moisture dynamics and related changes in effective stress and stress–strain behaviour [16,21–28]. One of the problems that is likely to worsen due to climate change and has been paid limited attention in the literature is reactive soil movement and its effects on shallow lightweight structures such as pavements, pipelines, or footings for residential buildings [29–33]. Approximately 30% of Australia’s surface soil can be classified as reactive (also known as expansive soils). These soils go through significant volume change due to changes in moisture content resulting in ground movement, which can influence the safety and serviceability of the structures built on them.

Leao [34] investigated the effect of changes in ground movement due to climate change on the residential footing for the state of Victoria, Australia and assessed the associated risks. One of the conclusions from their study was that most urban growth areas were susceptible to medium to high risk for damage. However, the focus of the study was limited to changes in climate from the years 2001 to 2011. Mitchell [31] discussed the importance of considering climate change in the design of structures on expansive soils and used the Thornthwaite Moisture Index (TMI) as a climate classifier in his study. The scope of his study, however, was limited to four capital cities of Australia (Adelaide, Melbourne, Sydney, and Perth). Yue [35] investigated different methods of calculating TMI and compared three different methods [36–38] and indicated that when using a TMI-based approach in predicting climate-related unsaturated soil parameters, caution should be exercised as large variabilities among correlations/results from different methods were observed. Karunarathne [33] and Karunarathne [30] investigated the effect of the atmospheric boundary interaction, how it may affect ground movement, and how the estimation procedure may influence the footing design. Sun et al. [32] assessed the effect of climate change on expansive soil movement and site classification. However, their study mainly focused on the state of Victoria and the five major cities of Australia. Several past studies [39–41] have also investigated the influence of atmospheric boundary interaction and climate change on the behaviour of lightweight structures such as road pavements on expansive soils. However, the findings may not directly translate to the Australian climate, more specifically the South Australian climate, as the studies were conducted for a different part of the world. There has been very limited research on the effect of climate change on expansive soils in South Australia. To the author’s best knowledge, no predictive TMI map exists for South Australia based on the most recent climate predictors that designers can use as a reference tool.

AS2870-2011 [42], the Australian standard relating to the design of footings for lightweight structures on expansive soils, provides a guideline for the estimation of the depth of design soil suction change (H_s) based on the TMI. H_s is the depth below which the short-term climatic variation on a built-up greenfield site does not affect the soil moisture content. Therefore, the soil below H_s does not contribute to ground movement. With knowledge of the soil profile and the rate of vertical strain for a unit change in suction for the various soils throughout the soil profile, the design soil suction changes for the site are used to estimate the potential differential ground movement, or design characteristic ground movement (y_s) [43]. This parameter influences the designed stiffness of the near-surface footing, which is required to maintain the serviceability of the supporting structure. Since TMI affects the depth of design suction changes, it indirectly affects footing design for footings built in/on expansive soils. TMI may have similar influences on other geotechnical structures. Therefore, prediction of the potential TMI changes in the coming future is necessary to ensure that infrastructure built today can last into the future [44,45]. Given that changes to temperature and rainfall caused by climate change will lead to changes in TMI, geotechnical designers must be adequately aware and prepare for such effects [46].

In this paper, the literature for three commonly used methods for calculating TMI is briefly discussed. Sixty-six years of weather data from a weather station in South Australia were used to calculate TMI using the methods discussed and compared. Based on the comparison, a selected method is used to calculate a set of “current TMI” values for 70 locations across South Australia and plotted in a GIS map. The “current TMI” calculation is based on the most recent 30 years of weather data from weather stations at the selected locations. Based on the forecasted changes in climate for the years 2050 and 2080 in different emission scenarios, a series of predictive TMI maps are also developed. A simplified methodology is developed to estimate the future changes in ground movement and implemented for a selected area of South Australia. A series of ground movement maps are produced representing current and different future climate scenarios. The consequence of these changes is also discussed using a simplified footing design example.

2. Methods for Estimating TMI

TMI, calculated as a function of rainfall and potential evapotranspiration, was first introduced in 1931 by Thornthwaite [47] and has been widely accepted and employed within the scientific community in many applications. Thornthwaite [36] initially applied TMI as a tool to map the climate zones of the United States of America, which was further extended in applications in the agricultural field as an indicator of suitable climates for various crop types [48]. TMI has also been used in other areas, including ecological community, prediction of water catchment capacities and forest growth, and estimation of potential soil suction beneath covered areas and pavements [49–51]. In Australia, TMI has been adopted to understand general differences in climate across the country [49,52] and estimate the depth of design soil suction changes H_s , which is needed to determine y_s [42].

Over several decades, various methods/equations have been developed to estimate TMI. The original method, developed by Thornthwaite [36], calculated TMI as,

$$TMI = I_h - 0.6I_a = \frac{100R - 60D}{PET} \quad (1)$$

where, I_h = humidity index = $100\left(\frac{R}{PET}\right)$; I_a = aridity index = $100\left(\frac{D}{PET}\right)$; R = moisture runoff or quantity of moisture that cannot be absorbed in an already wet site; D = moisture deficit; PET = potential evapotranspiration or the possible loss of moisture from the ground surface and vegetation. This method will be referred to as Method 1 from this point onward.

According to Method 1, I_h and I_a quantitatively captures the soil’s ability to store water between the extreme cases of completely dry and fully saturated states and could be used to distinguish extremes in seasonal moisture conditions, such as droughts and periods of prolonged rain. Method 1 also attempted to account for the effects of vegetation on the moisture balance. The 0.6 multiplier to the aridity index was introduced into the method to account for an assumption that water can enter the soil at a faster rate than it can be extracted from the soil profile [5,36,53]. This method requires estimation of (i) monthly moisture surplus— R , (ii) monthly moisture deficit— D , and (iii) monthly adjusted potential evapotranspiration— PET . The first two parameters (i.e., R and D) can be derived using a water balance approach and the calculation procedure has been described by McKeen and Johnson [54]. Empirical methods for calculating PET have evolved over the past decades; however, the common approach in the literature is by using the adjusted potential evapotranspiration for the month, i (PET_i) and can be determined by using the Thornthwaite [36] evapotranspiration equation as presented in Equation (2) below. The equation simply relies on precipitation and temperature data which are readily available from most of the weather stations.

$$PET_i = pe_i \left(\frac{D_i N_i}{30} \right) \quad (2)$$

here, D_i is the day length correction factor for the month i ; N_i is the number of days in the month i ; pe_i is the non-adjusted potential evapotranspiration for the month i and can be calculated as:

$$pe_i = 1.6 \times \left(\frac{10t_i}{H_y} \right)^a \quad (3)$$

where, (t_i) is the mean monthly temperature in °C of the study location for a given month (i) and can be calculated as the average of the minimum and maximum temperature. H_y is the yearly heat index and can be determined using t_i as:

$$H_y = \sum_{i=1}^{12} (0.2t_i)^{1.54} \quad (4)$$

where, y denotes the given year. The power term a in Equation (3) is a coefficient that ranges between $0 < a < 4.25$, and can be calculated as:

$$a = \left(6.75 \times H_y^3 \times 10^{-7} \right) - \left(7.71 \times H_y^2 \times 10^{-5} \right) + (0.01792 \times H_y) + 0.49239 \quad (5)$$

It is important to note that a positive value of TMI indicates a humid or wet climate with higher soil moisture, while a negative value of TMI represents an arid climate with less moisture in the soil. Zero TMI indicates there is no net soil moisture change for the study period. In other words, the soil moisture is in balance with environmental conditions.

Thornthwaite and Mather [37] modified the TMI equation by removing the coefficient of 0.6 for the aridity index, as shown in Equation 6, and this made the calculation process considerably simpler.

$$TMI = 100 \left(\frac{P}{\sum PET_i} - 1 \right) \quad (6)$$

here, P is the precipitation. Equation (6) will be referred to as Method 2 in this paper. Witzec et al. [38] further modified Method 2 as below,

$$TMI = 75 \left(\frac{P}{\sum PET_i} - 1 \right) + 10 \quad (7)$$

This method will be referred to as Method 3 in this paper.

3. Comparison of Methods 1, 2, and 3

A comparative study was conducted using the three methods discussed in the previous section. A total of 66 years of weather data (1955 to 2020) were collected from a weather station in Adelaide (Adelaide Airport, Lat. -34.95 degree, Long. 138.52 degree). Collected weather data included monthly rainfall, mean maximum, and mean minimum temperature. TMIs were calculated using the collected weather data and Methods 1, 2, and 3. The calculated TMIs from the different methods are presented in Figure 1 below. Significant differences could be observed between Method 1 and Method 2. Calculations from Method 1 and Method 3, however, were very close to each other. Provided that AS2870-2011 [42] uses Method 1 for TMI estimation and Method 3 is significantly simpler to apply yet produces results very close to Method 1, Method 3 was used for all further calculations of TMI in this study.

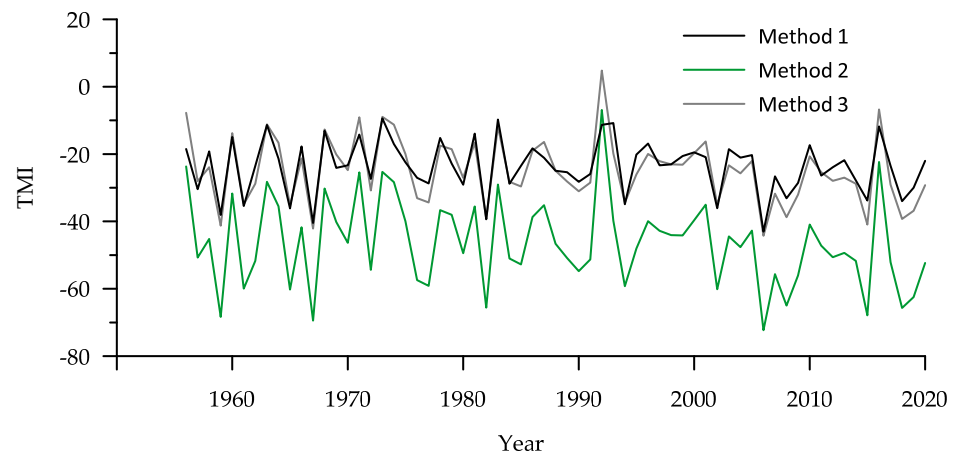


Figure 1. Calculated TMI values from Methods 1, 2, and 3 for a weather station in Adelaide.

4. Future Climate of South Australia

Climate Change Australia [6] presents a series of future climate scenarios for different regions (clusters) of Australia. The state of South Australia falls into three of those climate clusters, namely Rangelands, Southern and South-Western Flatlands, and Murray Basin. The climate clusters are shown in Figure 2. Tables 1 and 2 summarize the projected changes in temperature and rainfall respectively for different emission scenarios for 2050 and 2080. Three different emission scenarios, i.e., representative concentration pathways RCP2.6, RCP4.5, and RCP8.5 are summarized here. RCP2.6 assumes the greenhouse gas emission peaking around the year 2020 and then declining rapidly. The CO₂ concentration in the atmosphere is expected to reach 440 ppm by 2040 and then reduce to 420 by the end of the 21st century. RCP4.5 assumes the emission to peak around 2040 and the CO₂ concentration to reach 540 ppm by the year 2100. RCP8.5 is the most pessimistic scenario where minor changes in the current emission trend are assumed and CO₂ rises to 660 ppm by the end of this century [55].

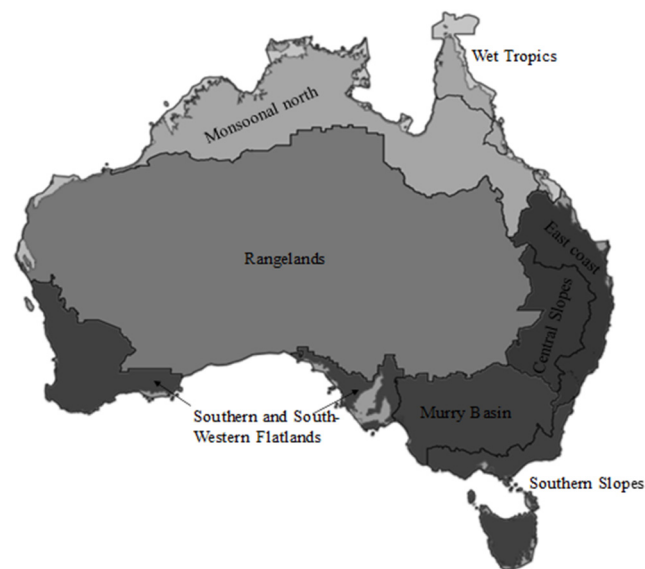


Figure 2. Climate clusters of Australia [6].

Table 1. Summary of predicted temperature changes (°C) for different climate clusters and different emission scenarios; data from Climate Change Australia (2020).

Year	Rangelands			Southern and South-Western Flatlands			Murray Basin		
	RCP 2.6	RCP 4.5	RCP 8.5	RCP 2.6	RCP 4.5	RCP 8.5	RCP 2.6	RCP 4.5	RCP 8.5
2050	1.1	1.5	1.9	0.8	1.2	1.5	0.95	1.2	1.7
2080	1.1	2.1	4.2	0.8	1.7	3.3	0.95	1.8	3.7

Table 2. Summary of predicted rainfall changes (% relative to 1986 to 2005 average) for different climate clusters and different emission scenarios; data deduced from Climate Change Australia [6].

	Rangelands			Southern and South-Western Flatlands			Murray Basin		
	RCP2.6	RCP4.5	RCP8.5	RCP2.6	RCP4.5	RCP8.5	RCP2.6	RCP4.5	RCP8.5
Year 2050									
Summer	−4	1	−1	−3.5	−1	−5	−5	4	1
Autumn	0	1	0.5	−3	−4	−3	−1	−1.2	−5.5
Winter	−7	−10	−12.5	−6	−11	−15	−1.5	−5	−4
Spring	−7	−3	−5	−8	−10.5	−16	−2	−4	−5
Average	−4.5	−2.8	−4.5	−5.1	−6.6	−9.8	−2.38	−1.6	−3.4
Winter/spring avg.	−7	−6.5	−8.75	−8	−10.5	−16	−2	−4	−5
Year 2080									
Summer	−5	−3	2	−8	−3.8	−4	−1	−1.5	6.5
Autumn	−5	0	7	−3	−4	−3	−4	3.5	0
Winter	−4	−11	−20	−7	−13.5	−26	−2	−8	−12
Spring	−5	−10	−11	−9	−16	−32	−4	−11	−12
Average	−4.8	−6.0	−5.5	−6.8	−9.3	−16.3	−2.75	−4.3	−4.4
Winter/spring avg.	−5	−10	−11	−9	−16	−32	−4	−11	−12

Under different emission scenarios, the temperature of different regions of South Australia has been predicted to rise by 0.8 to 1.9 °C by 2050 and by 0.95 to 4.2 °C by 2080. In most areas of South Australia, the rainfall is expected to decrease in all seasons of the year, with the maximum reduction expected in winter and spring. It is to be noted that Climate Change Australia [6] provides the probabilistic changes in rainfall and temperature pattern; the numbers presented here are deduced average values.

5. TMI Map of South Australia for Current and Future Climate Scenarios

TMI is an annual index and is calculated from monthly historical data. It can be calculated for a particular location for any specific year, as shown in Section 3 of this paper, and this approach is generally known as the year-by-year method. An alternative to the year-by-year method is to assemble monthly average temperatures and rainfalls using all existing data and calculate TMI for a single average year. This method is known as average year analysis. For simplifying the calculation, an average year approach was used in this paper. The calculation steps are outlined below,

- (1). The mean temperature for each month of the year was determined by averaging the maximum and minimum monthly temperatures over 30 years for that particular month.
- (2). The heat index for each month was then calculated using Equations (4) and (5).
- (3). The next step involved the calculation of unadjusted potential evapotranspiration using Equation (3).
- (4). Calculated unadjusted values of potential evapotranspiration were then adjusted for day length using Equation (2). The day length correction factors for relevant latitudes are presented in Table 3.
- (5). TMI was calculated using Equation (7).

Table 3. Day length correction factor (D_i) for each month.

Lat. (deg)	Jan	Feb	Mar	Apr	May	Jun	Jul	Aug	Sep	Oct	Nov	Dec
20	1.14	1.00	1.05	0.97	0.96	0.91	0.95	0.99	1.00	1.08	1.09	1.15
25	1.17	1.01	1.05	0.96	0.94	0.88	0.93	0.98	1.00	1.10	1.11	1.18
30	1.20	1.03	1.06	0.95	0.92	0.85	0.90	0.96	1.00	1.12	1.14	1.21
35	1.23	1.04	1.06	0.94	0.89	0.82	0.87	0.94	1.00	1.15	1.17	1.25
40	1.27	1.06	1.07	0.93	0.86	0.78	0.84	0.92	1.00	1.15	1.20	1.29

The past 30 years of weather data (1991 to 2020) from 70 weather stations scattered across South Australia were used for this exercise, and the calculated set of TMI values were tagged as “Current TMI”. Using GIS software, the “Current TMI” data were plotted in a contour map with contour intervals of 10. The map is presented in Figure 3a with the city of Adelaide and surrounding areas highlighted.

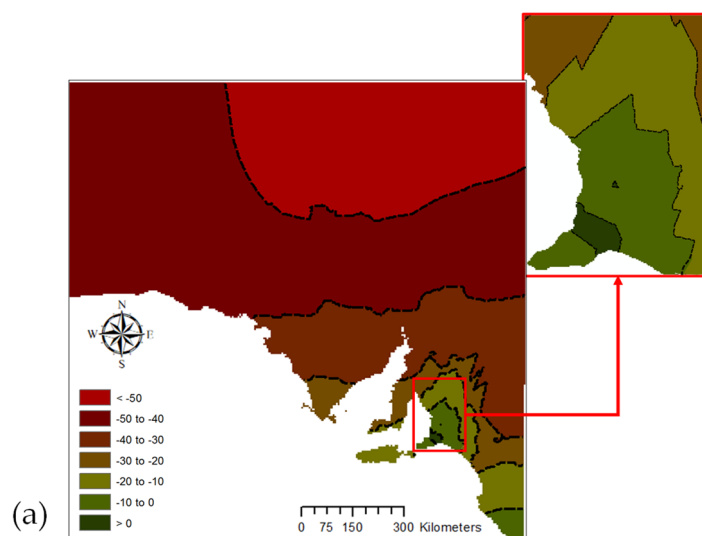


Figure 3. Cont.

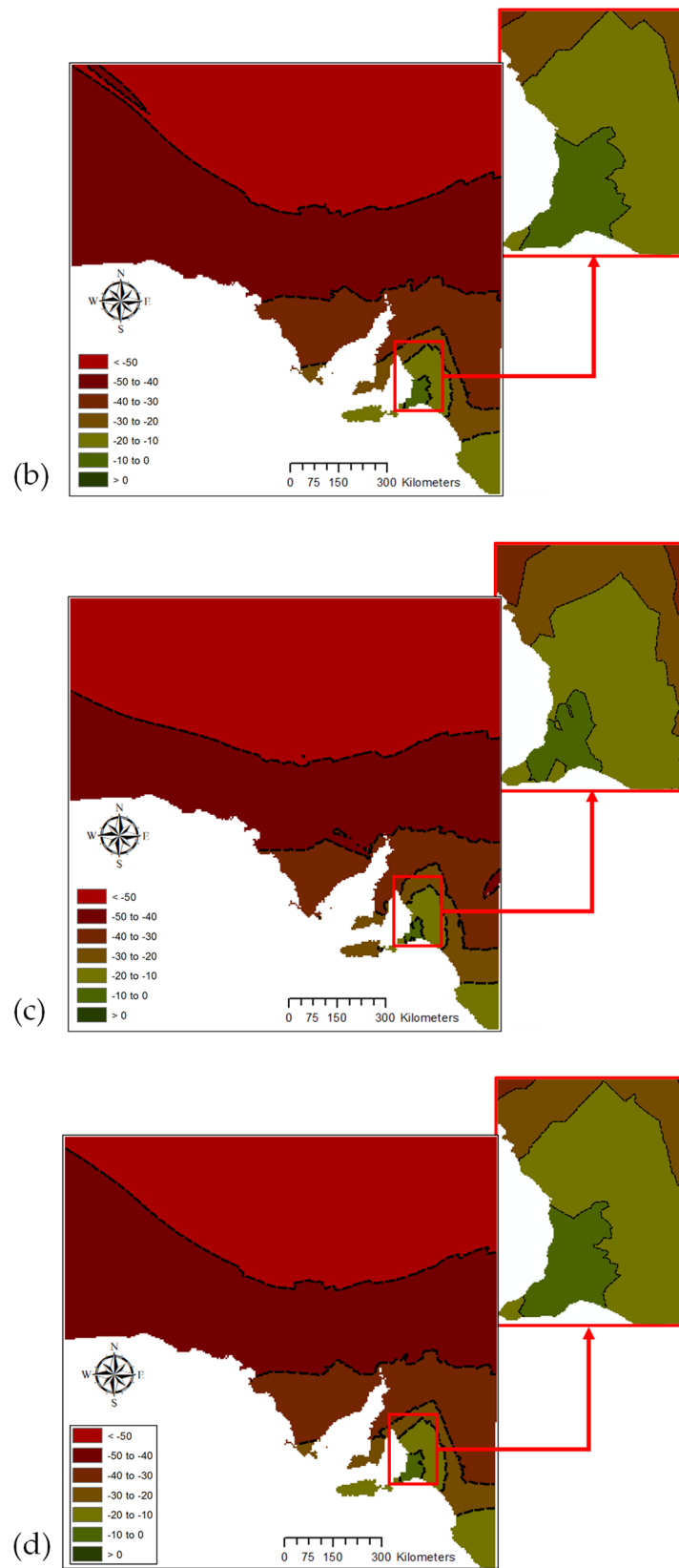


Figure 3. Cont.

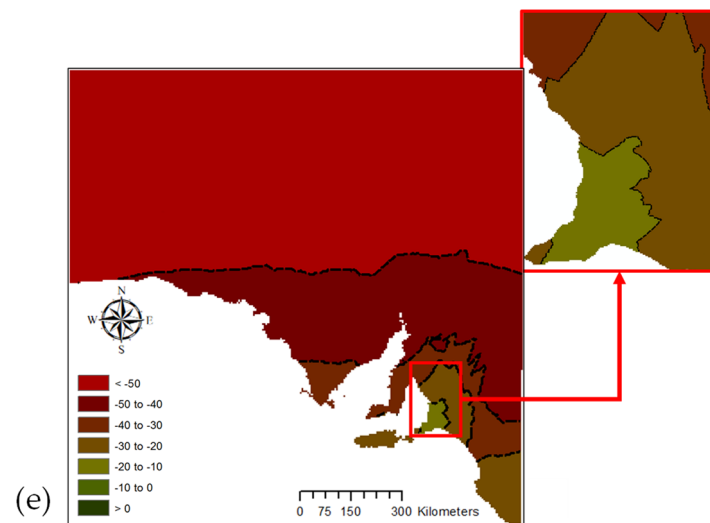


Figure 3. TMI maps of South Australia with Adelaide area highlighted under (a) current climate, (b) 2050 low emission scenario, (c) 2050 high emission scenario, (d) 2080 low emission scenario, and (e) 2080 high emission scenario.

Four other sets of TMI values were calculated for 2050 low, 2050 high, 2080 low, and 2080 high emission scenarios. The TMI map for the 2050 low emission scenario was developed based on an average temperature increase of $0.95\text{ }^{\circ}\text{C}$ and a 4% reduction in rainfall (yearly average across the three clusters for RCP 2.6) applied to the past 30 years of average monthly temperature and rainfall data, respectively. That is, an average monthly temperature increase of $0.95\text{ }^{\circ}\text{C}$ was added and a 4% rainfall was deducted from the past 30 years monthly average data.

Similarly, the 2050 high emission scenario was based on a $1.72\text{ }^{\circ}\text{C}$ rise in temperature accompanied by a 5.9% reduction in rainfall. The 2080 high and low scenario TMIs were calculated based on 0.98 and $3.75\text{ }^{\circ}\text{C}$ rises in temperature and 4.75 and 8.7% reduction in rainfall, respectively, related to RCP2.6 and RCP8.5 climate change scenarios. The predictive TMI maps for 2050 and 2080 are presented in Figure 3b–e. Calculated TMI values for all weather station locations are presented in Table 1 in Appendix A at the end of this paper.

The comparison exercise (see Figure 3a–e) indicates that the South Australian climate is likely to get drier under all four future climate scenarios considered here. An average (average values from all 70 weather stations) TMI change of -3.4 was observed for the 2050 low emission scenario, which increased to -5.5 in the high emission scenario for the same year. For 2080, the average changes were -3.6 and -10.4 for high and low emission scenarios, respectively. The average TMI values for South Australia along with average changes and minimum and maximum values are summarized in Table 4 below. One interesting observation could be made from Table 4 and Appendix A that the areas with relatively wetter climates (higher TMI) are affected more significantly (in future climate scenarios) compared to areas with lower TMI under the current climate.

It is difficult to quantify the changes with a high degree of certainty as climate change is a function of a range of different factors. However, the developed maps are indicative of future changes and engineers working on design projects should accommodate these changes in their current design if the structure is expected to last over its design life, for example, 50 or 100 years.

Table 4. Average, average change, minimum, and maximum TMI values calculated for South Australia under different climate scenarios.

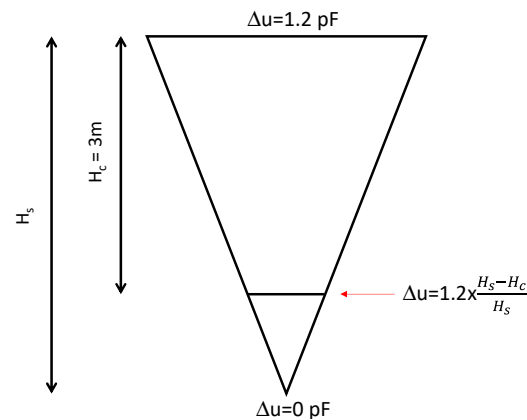
	Current	2050 Low Emission	2050 High Emission	2080 Low Emission	2080 High Emission
Average TMI	−25.3	−28.7	−30.8	−28.9	−35.7
Average change	—	−3.3	−5.5	−3.6	−10.4
Minimum TMI	−55.9	−57.1	−57.9	−57.1	−59.7
Maximum TMI	51.4	42.8	37.5	42.1	26.3

6. Changes in Ground Movement in a Local Government area of South Australia

The characteristic expansive soil movement was calculated using a simplified method. According to AS 2870-2011 [42], for Adelaide and surrounding areas, the changes in suction at the soil surface between driest and wettest points on an allotment over the structure's design life (Δu) can be taken as 1.2 pF, and the depth of cracking (H_c) can be taken as 3 m. A triangular distribution of soil suction changes then can be assumed, which extends to the depth H_s as shown in Figure 4 below. AS2870-2011 [42] provides guidelines that can be used for estimating H_s based on TMI of a particular area. The characteristic ground movement, y_s can be calculated as,

$$y_s = \Delta z \Delta u (\alpha I_{ps}) \quad (8)$$

were, $\alpha = 2 - z/5$ above H_c , and $\alpha = 1$ below H_c ; z is the depth, I_{ps} is the soil reactivity. α takes into account the degree of lateral confinement and to some extent overburden pressure.

**Figure 4.** Soil suction change profile.

For this exercise, a town centre and surrounding area in South Australia (not named here) was selected based on data availability. A soil reactivity database of 135 locations within the selected area was created based on a published soil movement map [56]. H_s was estimated for each of the 135 data points based on the corresponding location's TMI for the "current" climate scenario using a correlation established from AS2870 [42]. The same exercise was repeated for 2050 low and 2080 high emission future climate scenarios. Based on the estimated H_s and using Equation (8), y_s was calculated for each of the 135 locations for each of the different climate scenarios.

The soil movement map developed based on H_s estimated from current TMI values is presented in Figure 5a. It is to be noted that only the effect of changes in climate on H_s was considered in this exercise and the changes in Δu was ignored to avoid complexity and lack of reliable methods to calculate them. Increased temperature and reduced rainfall are likely to increase Δu for many soil types and thus ignoring this may have contributed to some underestimation of y_s in the current exercise.

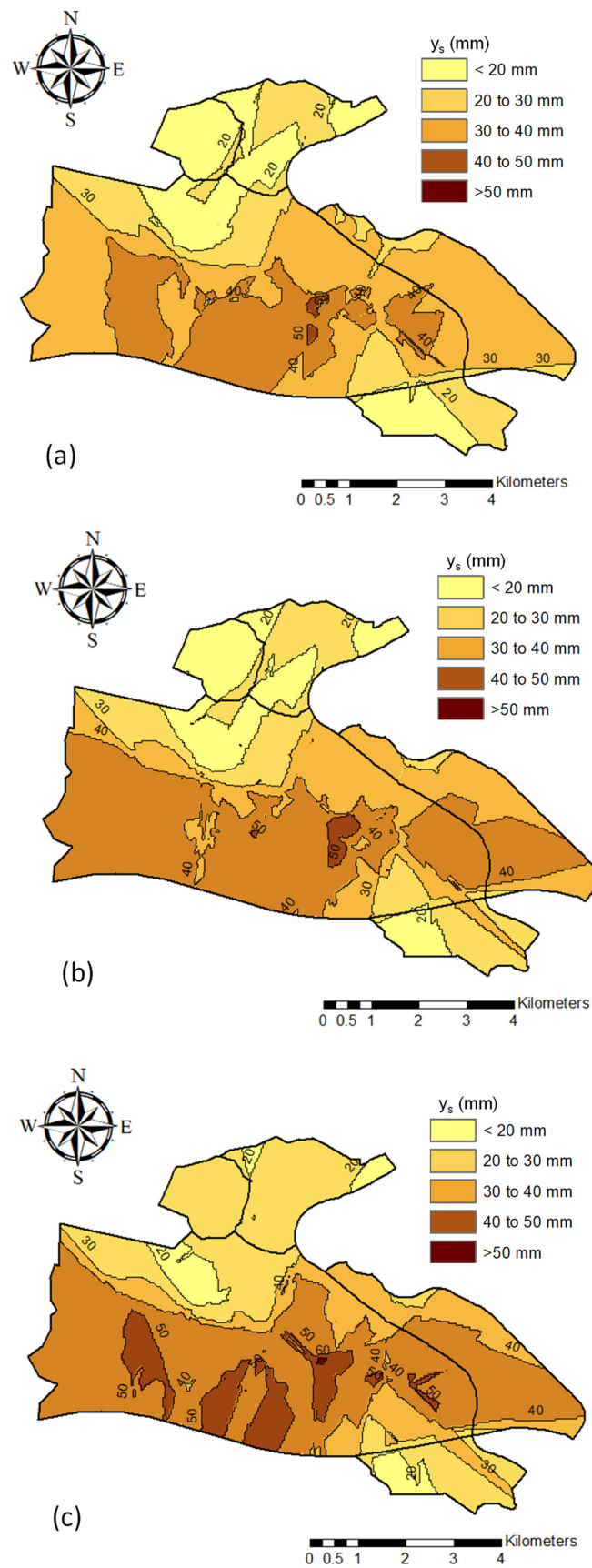


Figure 5. Characteristic ground movement maps for (a) current climate, (b) 2050 low emission scenario, and (c) 2080 high emission scenario.

Figure 5a shows that majority of the study area under the current climate has y_s less than 40 mm. According to AS2870 [42], these sites can be classified as slightly to moderately reactive clay or silt sites with deep-seated moisture changes. A small proportion of the area has $y_s > 40$ mm with an even smaller proportion of the area with $y_s > 50$ mm. AS2870 [42] considers these sites to be experiencing high to very high ground movement.

In Figure 5b,c, the y_s for the same area under 2050 low emission and 2080 high emission scenarios are presented. y_s values have been calculated using a similar approach as Figure 5a but with H_s calculated based on changed TMI. The average H_s increased by 0.17 m and 0.51 m respectively for 2050 low and 2080 high emission scenarios resulting in significant changes in y_s in the two forecast movement maps. The area with $y_s < 40$ mm reduced significantly with an accompanying increase in areas with larger movement potential. The area with $y_s > 50$ mm which was limited to less than approximately 1% of the investigated area under the current climate scenario, increased by approximately 10-fold in the 2080 high emission scenario.

On average the y_s values increased by 4.6% and 13.4% with maximum changes of 4.23 and 12.2 mm for 2050 low and 2080 high emission scenarios respectively. Increased ground movement potential will mean structures built on such sites will have to cope with additional stresses exerted to them by the soil due to seasonal variations in moisture in soils and may fail if the expected future changes are not incorporated in their design.

To highlight the possible implication of the changes in ground movement, a hypothetical case is discussed here. A rectangular stiffened raft footing (15 m \times 10 m) with three and four beams in the long and short directions, respectively) is designed for a lightweight residential building on an expansive soil site characterized by y_s of 50 mm under the current climate. The design exercise is repeated for a possible future scenario where a 10 mm increase in y_s is expected. It is to be noted that in the design of shallow footings for lightweight structures on reactive soil sites, the conventional method based on bearing capacity principles do not apply. The design is dictated by stresses applied to footing structures by expansive soil movement and works on the principle of limiting the differential movement of the footing structure within the tolerance of the superstructure. The design inputs are summarized in Table 5 below. A computer program CORD [57] which incorporates the Walsh method [58,59] for estimating the mound shape was used for the design.

A stiffened slab designed under the current climate scenario would require 300 mm beam depth for an articulated masonry veneer type superstructure. For a 10 mm increase in ground movement, the design for the same superstructure will require a beam depth of 380 mm and a slightly higher reinforcement area.

The analysis indicates, for geotechnical structures where soil-atmospheric boundary interaction significantly affects the stability, the changes in climate need to be taken into account. Using the methodology outlined here, tools can be developed to estimate expected future soil movements and incorporated into the design rather than using soil's current movement potential. The maps presented here can also assist in the establishment of policies and strategies towards the development of resilient infrastructure.

It should be noted that the extrapolation used in estimating the ground movement may not be very accurate as they are based on gross approximation and can be argued upon and certainly requires further research and refinement. To estimate the effect of future climate, the changes in temperature and rainfall have simply been added to the past 30 years' average values. This can be looked at as an oversimplification of the interaction that occurs at the soil-vegetation-atmosphere boundary. However, the change in suction depth is a seasonal process and is contributed to by incremental changes due to the soil-atmospheric boundary interactions over months (often 6 months, i.e., the difference in time between the end of summer to the end of winter). The current methodology cannot capture the effect of individual weather events explicitly especially considering more intense but shorter duration heavy rainfall will be a feature of the future climate of Australia. However, considering the suction depth changes occurs over a long time, the assumptions can be treated

as reasonable. Nonetheless, it highlights the importance of incorporating/accommodating climate change-related effects on the designs of geotechnical structures today, especially those located at shallow depths such as pipelines, pavements, and so forth.

Table 5. Design details for a rectangular footing on reactive soil.

Size of footing	15 m × 10 m
Number of beams in the longitudinal direction	3
Number of beams in the transverse direction	4
Slab thickness	100 mm
Clear cover	20 mm
Slab live load	0.75 kPa
Slab reinforcement	179 mm ² /m
Beam width	300 mm
Beam depth	being designed
Concrete strength	25 MPa
Roof type	Conventional sheet (0.45 kPa)
Wall height	2.4 m
Wall weight (external)	2.5 kN/m ²
Wall weight (internal)	0.5 kN/m ²
Beam bottom reinforcement (current climate scenario)	2 × 12 mm
Beam top reinforcement (current climate scenario)	none

7. Conclusions

The followings are the conclusions from this study,

- An increase in temperature and reduction in rainfall will be the feature of the future climate in South Australia with a 0.8 to 4.2 °C rise in temperature and up to 16.3% reduction in average rainfall in different parts of South Australia under different emission scenarios.
- TMI maps for “current” and four future climate scenarios have been developed for South Australia that can be used as a reference by designers for making informed decisions when designing on reactive soils.
- The average change in TMI across South Australia was estimated to be −3.4 in the 2050 low emission scenario (RCP2.6) which can increase to −10.4 under the 2080 high emission scenario (RCP8.5).
- The estimated changes in TMI were not uniform across South Australia. The areas with high TMI values under the current climate were the worst affected and vice versa.
- Changes in TMI will lead to significant changes in ground movement. The maximum increase in the potential ground movement was calculated to be 4.23 and 12.2 mm for 2050 low and 2080 high emission scenarios respectively.
- A hypothetical exercise comparing two foundation designs, one under current climate and one under future climate scenario, showed that the changes in characteristic ground movement may lead to premature failure of structure as the design may be deemed inadequate and demonstrated the importance of incorporating the climate change in the design of geotechnical structures especially the lightweight structures founded within the depth of suction change.

Author Contributions: Conceptualization, M.R.K. and M.M.R.; methodology: M.R.K., D.C., and K.N.; formal analysis K.N., A.I., and I.A.; data curation M.R.K.; writing—original draft preparation, M.R.K. and K.N.; writing—review and editing M.M.R., D.C., and I.A.; visualization A.I. and K.N.; project administration M.R.K. All authors have read and agreed to the published version of the manuscript.

Funding: This research received no external funding.

Institutional Review Board Statement: Not applicable.

Informed Consent Statement: Not applicable.

Data Availability Statement: Weather data can be downloaded free of cost from Bom.gov.au. Interested readers can contact the authors of this paper for more details.

Conflicts of Interest: The authors declare no conflict of interest.

Disclaimer: The opinion expressed in this paper are of the authors and the assumptions must be understood and engineering judgement should be used for its use in any design or other purpose.

Appendix A

Table 1. Calculated TMI values for 70 weather stations in South Australia.

Site Name	Latitude	Longitude	Current	2050 Low	2050 High	2080 Low	2080 High
Nullarbor	−31.4492	130.8976	−42.4	−44.4	−45.7	−44.5	−48.7
Ceduna amo	−32.1297	133.6976	−37.5	−39.9	−41.5	−40.1	−45.1
Elliston	−33.6501	134.888	−29.7	−32.7	−34.6	−32.9	−39.1
North shields (Port Lincoln aerodrome)	−34.6017	135.8732	−24.9	−28.2	−30.4	−28.5	−35.4
Cleve	−33.7011	136.4937	−28.0	−31.2	−33.3	−31.4	−38.1
Whyalla Aero	−33.0539	137.5205	−41.9	−44.0	−45.4	−44.1	−48.7
Port Augusta power station	−32.528	137.79	−45.0	−47.0	−48.4	−47.1	−51.6
Kadina Aws	−33.9703	137.6628	−33.6	−36.4	−38.2	−36.6	−42.5
Maitland	−34.3745	137.6733	−18.1	−22.2	−24.8	−22.5	−30.9
Minlaton Aero	−34.748	137.5276	−32.1	−35.0	−36.9	−35.2	−41.1
Stenhouse Bay	−35.2795	136.9392	−23.4	−26.9	−29.2	−27.2	−34.4
Warooka	−34.9906	137.3995	−23.1	−26.6	−28.9	−26.9	−34.2
Edithburgh	−35.1121	137.7395	−29.1	−32.1	−34.1	−32.4	−38.5
Price	−34.2971	138.0014	−34.3	−36.9	−38.7	−37.1	−42.6
Edinburgh RAAF	−34.7111	138.6222	−25.8	−29.3	−31.6	−29.6	−36.8
Parafield airport	−34.7977	138.6281	−23.9	−27.5	−29.9	−27.8	−35.4
Adelaide (Kent town)	−34.9211	138.6216	−16.2	−20.6	−23.5	−20.9	−30.2
Adelaide airport	−34.9524	138.5204	−23.8	−27.3	−29.6	−27.6	−34.9
Mount Lofty	−34.9784	138.7088	51.4	42.8	37.5	42.1	26.3
Noarlunga	−35.1586	138.5057	−23.6	−27.3	−29.7	−27.6	−35.3
Kuitpo forest reserve	−35.1712	138.6783	7.1	1.3	−2.3	0.9	−10.4
Myponga	−35.3912	138.4642	15.6	9.4	5.6	8.9	−2.8
Parawa (Second valley forest aws)	−35.5695	138.2864	23.5	16.7	12.5	16.2	3.2

Table 1. Cont.

Site Name	Latitude	Longitude	Current	2050 Low	2050 High	2080 Low	2080 High
Victor Harbor (Encounter bay)	−35.5544	138.5997	−10.6	−14.9	−17.7	−15.3	−24.0
Hindmarsh Island awes	−35.5194	138.8177	−27.6	−30.7	−32.7	−30.9	−37.4
Meningie	−35.6902	139.3375	−19.0	−22.7	−25.1	−23.0	−30.5
Cape Jaffa (the limestone)	−36.9655	139.7164	−14.1	−18.1	−20.6	−18.4	−26.2
Robe airfield	−37.1776	139.8054	−2.9	−7.7	−10.7	−8.1	−17.5
Mount gambier Aero	−37.7473	140.7739	10.9	5.1	1.5	4.7	−6.3
Coonawarra	−37.3	140.8333	−6.6	−11.2	−14.0	−11.5	−20.4
Struan	−37.0951	140.7911	−8.5	−12.9	−15.7	−13.3	−21.9
Naracoorte Aerodrome	−36.9813	140.727	−16.4	−20.3	−22.8	−20.6	−28.3
Lucindale post office	−36.9731	140.3664	−4.1	−8.9	−12.0	−9.3	−18.9
Padthaway South	−36.6539	140.5212	−19.8	−23.4	−25.7	−23.7	−31.0
Keith	−36.098	140.3556	−20.6	−24.3	−26.7	−24.6	−32.1
Lameroo (Austin plains)	−35.3778	140.5378	−35.3	−37.8	−39.5	−38.0	−43.3
Tailem Bend	−35.2546	139.4542	−29.5	−32.5	−34.4	−32.7	−38.8
Murray Bridge	−35.1167	139.2667	−32.4	−35.2	−37.0	−35.4	−41.2
Strathalbyn	−35.256	138.8901	−16.6	−20.6	−23.1	−20.9	−28.8
Mount Barker	−35.073	138.8465	14.5	8.3	4.4	7.8	−4.2
Lenswood research centre	−34.9482	138.8071	41.4	33.2	28.0	32.5	16.5
Karoonda	−35.09	139.8972	−33.3	−36.1	−37.9	−36.3	−42.0
Caliph	−34.6345	140.2432	−39.7	−41.9	−43.3	−42.0	−46.5
Loxton research centre	−34.439	140.5978	−41.0	−43.1	−44.5	−43.3	−47.6
Renmark Aero	−34.1983	140.6766	−43.9	−45.9	−47.2	−46.0	−50.1
Gluepot reserve (Gluepot)	−33.7622	140.1251	−40.2	−42.5	−44.0	−42.7	−47.5
Nuriootpa Viticultural	−34.4761	139.0056	−21.0	−24.6	−27.0	−24.9	−32.4
Rosedale (Turretfield research centre)	−34.5519	138.8342	−21.5	−25.3	−27.7	−25.5	−33.3
Kapunda	−34.3412	138.9155	−17.8	−21.7	−24.3	−22.0	−30.1
Eudunda	−34.1754	139.0847	−21.0	−24.6	−27.0	−24.9	−32.2
Gammon ranges (Balcanoona)	−30.5328	139.3029	−47.2	−49.0	−50.2	−49.1	−53.0
Arkaroola	−30.311	139.3357	−44.7	−46.8	−48.2	−47.0	−51.5
Moomba airport	−28.0997	140.1956	−55.3	−56.6	−57.5	−56.7	−59.6
Mount Dare	−26.0702	135.2471	−54.4	−55.7	−56.6	−55.8	−58.7
Ernabella (Pukatja)	−26.2635	132.1771	−45.7	−47.9	−49.4	−48.0	−52.8
Marla police station	−27.3002	133.6201	−50.1	−51.9	−53.1	−52.0	−56.0
Oodnadatta airport	−27.5553	135.4456	−54.6	−55.9	−56.9	−56.0	−59.0
Cooper Pedy	−29.004	134.7564	−54.4	−55.6	−56.5	−55.7	−58.4
Cook	−30.6143	130.4136	−49.4	−50.9	−51.9	−51.0	−54.1

Table 1. Cont.

Site Name	Latitude	Longitude	Current	2050 Low	2050 High	2080 Low	2080 High
Maralinga	−30.1591	131.579	−46.6	−48.4	−49.6	−48.5	−52.4
Tarcoola Aero	−30.7051	134.5786	−51.8	−53.3	−54.3	−53.4	−56.6
Wudinna Aero	−33.043	135.4519	−37.0	−39.6	−41.4	−39.8	−45.4
Kimba	−33.1416	136.4126	−33.9	−36.7	−38.5	−36.9	−42.8
Yudnapinna	−32.1232	137.1505	−47.8	−49.5	−50.6	−49.6	−53.2
Wilpena pound	−31.5286	138.6093	−23.6	−27.2	−29.5	−27.4	−34.9
Leigh Creek airport	−30.5963	138.4219	−48.3	−50.2	−51.4	−50.3	−54.3
Marree aero	−29.6587	138.0684	−55.9	−57.1	−57.9	−57.1	−59.7
Cape willoughby	−35.8426	138.1327	−11.4	−15.6	−18.3	−15.9	−24.5
Kingscote	−35.656	137.6377	−16.1	−19.9	−22.4	−20.2	−28.0
Cape Borda	−35.7549	136.5959	−8.7	−13.2	−16.1	−13.5	−22.5

References

- BOM. *State of the Climate 2018*. Available online: <http://www.bom.gov.au/state-of-the-climate/future-climate.shtml> (accessed on 2 November 2020).
- Cai, W.; Cowan, T. SAM and regional rainfall in IPCC AR4 models: Can anthropogenic forcing account for southwest Western Australian winter rainfall reduction? *Geophys. Res. Lett.* **2006**, *33*, L24708. [CrossRef]
- Cai, W.; Cowan, T. Southeast Australia Autumn Rainfall Reduction: A Climate-Change-Induced Poleward Shift of Ocean? Atmosphere Circulation. *J. Clim.* **2013**, *26*, 189–205. [CrossRef]
- Smith, I.N.; McIntosh, P.; Ansell, T.J.; Reason, C.J.C.; McInnes, K. Southwest Western Australian winter rainfall and its association with Indian Ocean climate variability. *Int. J. Climatol.* **2000**, *20*, 1913–1930. [CrossRef]
- Sun, X. The impact of climate as expressed by Thornthwaite moisture index on residential footing design on expansive soil in Australia. In *Civil Environmental and Chemical Engineering*; RMIT University: Melbourne, Australia, 2015.
- Climate Change Australia. *Climate Change in Australia*. Available online: <https://www.climatechangeinaustralia.gov.au/en/> (accessed on 2 November 2020).
- BOM. *Climate Change—Trends and Extremes; 2020* [cited 2020 10/11/2020]. Available online: <http://www.bom.gov.au/climate/change/#tabs=Tracker&tracker=trend-maps&tQ=map%3Dtmean%26area%3Daus%26season%3D0112%26period%3D1910> (accessed on 10 November 2020).
- Turner, S. *Climate Change Blamed as Landslip Incidents Treble*. New Civil Engineer 2001. Available online: <https://www.newcivilengineer.com/climate-change-blamed-as-landslip-incidents-treble/812153.article> (accessed on 1 July 2015).
- Ridley, A.; McGinnity, B.; Vaughan, P.R. Role of Pore Water Pressures in Embankment Stability. *Proc. Inst. Civ. Eng.* **2004**, *157*, 193–198. [CrossRef]
- Ng, P.B.; Poh, K.K.; Tenando, E. Slope failure after prolonged rainfall. In *BCA Seminar- Approach to Structural Inspection and Slope Stability*; Building and Construction Authority: Singapore, 2007.
- Hughes, P.N.; Glendinning, S.; Mendes, J.; Parkin, G.; Toll, D.G.; Gallipoli, D.; Miller, P.E. Full-scale testing to assess climate effects on embankments. *Proc. Inst. Civ. Eng. Eng. Sustain.* **2009**, *162*, 67–69. [CrossRef]
- Harley, R.; Sivakumar, V.; Hughes, D.; Karim, M.R.; Barbour, S.L. Progressive deformation of glacial till due to viscoplastic straining and pore pressure variation. In *Proceedings of the 67th Canadian Geotechnical Conference, Regina, SK, Canada, 28 September–1 October 2014*.
- Hughes, D. Monitoring the stability of infrastructure slopes in Northern Ireland to assess risk, using a combination of lidar, real-time dGPS, pore water pressures and geophysics. In *Proceedings of the 16th European conference on Soil Mechanics and Geotechnical Engineering, Edinburgh, UK, 13–17 September 2015*.
- Glendinning, S.; Helm, P.R.; Rouainia, M.; Stirling, R.A.; Asquith, J.D.; Hughes, P.N.; Toll, D.G.; Clarke, D.; Hudson, A.; Powrie, W.; et al. *Infrastructure Slopes: Sustainable Management And Resilience Assessment: iSMART-Final report*. EPSRC project EP/K027050/1, UK, 2018.
- Karim, M.R.; Hughes, D.; Rahman, M.M. Estimating hydraulic conductivity assisted with numerical analysis for unsaturated soil—A case study. *Geotech. Eng. J. SEAGS AGSSEA* **2020**, *52*, 12–19.
- Karim, M.R.; Hughes, D.; Kelly, R.; Lynch, K. A rational approach for modelling the meteorologically induced pore water pressure in infrastructure slopes AU—Karim, Md Rajibul. *Eur. J. Environ. Civ. Eng.* **2019**, *24*, 2361–2382. [CrossRef]
- Gatto, M.P.A.; Montrasio, L.; Berardengo, M.; Vanali, M. Experimental Analysis of the Effects of a Polyurethane Foam on Geotechnical Seismic Isolation. *J. Earthq. Eng.* **2020**, 1–22. [CrossRef]

18. Gatto, M.P.A.; Lentini, V.; Castelli, F.; Montrasio, L.; Grassi, D. The Use of Polyurethane Injection as a Geotechnical Seismic Isolation Method in Large-Scale Applications: A Numerical Study. *Geosciences* **2021**, *11*, 201. [[CrossRef](#)]
19. Ahenkorah, I.; Rahman, M.M.; Karim, M.R.; Beecham, S.; Saint, C. A review of Enzyme Induced Carbonate Precipitation (EICP): The role of enzyme kinetics. *Sustain. Chem.* **2021**, *2*, 92–114. [[CrossRef](#)]
20. Rahman, M.M.; Hora, R.N.; Ahenkorah, I.; Beecham, S.; Karim, M.R.; Iqbal, A. State-of-the-Art Review of Microbial-Induced Calcite Precipitation and Its Sustainability in Engineering Applications. *Sustainability* **2020**, *12*, 6281. [[CrossRef](#)]
21. Blight, G. The vadose zone soil-water balance and transpiration rates of vegetation. *Geotechnique* **2003**, *53*, 55–64. [[CrossRef](#)]
22. Briggs, K.M.; Smethurst, J.A.; Powrie, W.; O'Brien, A.S.; Butcher, D.J.E. Managing the extent of tree removal from railway earthwork slopes. *Ecol. Eng.* **2013**, *61*, 690–696. [[CrossRef](#)]
23. Smethurst, J.A.; Clarke, D.; Powrie, W. Factors controlling the seasonal variation in soil water content and pore water pressures within a lightly vegetated clay slope. *Géotechnique* **2012**, *62*, 429–446. [[CrossRef](#)]
24. Smethurst, J.; Briggs, K.M.; Powrie, W.; Ridley, A.; Butcher, D.J.E. Mechanical and hydrological impacts of tree removal on a clay fill railway embankment. *Geotechnique* **2015**, *65*, 869–882. [[CrossRef](#)]
25. Hughes, D.; Karim, M.R.; Briggs, K.; Glendinning, S.; Toll, D.; Dijkstra, T.; Powrie, W.; Dixon, N. A comparison of numerical modelling techniques to predict the effect of climate on infrastructure slopes. In *Geotechnical Engineering for Infrastructure and Development—Proceedings of the XVI European Conference on Soil Mechanics and Geotechnical Engineering, ECSMGE 2015*; ICE Publishing: London, UK, 2015.
26. Khalili, N.; Geiser, F.; Blight, G.E. Effective stress in partially saturated soils, a review with new evidence. *Int. J. Geomech.* **2004**, *4*, 115–126. [[CrossRef](#)]
27. Khalili, N.; Khabbaz, M.H. A unique relationship for χ for the determination of the shear strength of unsaturated soils. *Géotechnique* **1998**, *48*, 681–687. [[CrossRef](#)]
28. Fredlund, D.G. Unsaturated Soil Mechanics in Engineering Practice. *J. Geotech. Geoenvironmental Eng.* **2006**, *132*, 286–321. [[CrossRef](#)]
29. Teodosio, B.; Baduge, K.S.K.; Mendis, P. Simulating reactive soil and substructure interaction using a simplified hydro-mechanical finite element model dependent on soil saturation, suction and moisture-swelling relationship. *Comput. Geotech.* **2020**, *119*, 103359. [[CrossRef](#)]
30. Karunarathne, A.M.A.N.; Fardipour, M.; Gad, E.F.; Rajeev, P.; Disfani, M.M.; Sivanerupam, S.; Wilson, J.L. Modelling of Climate Induced Moisture Variations and Subsequent Ground Movements in Expansive Soils. *Geotech. Geol. Eng.* **2018**, *36*, 2455–2477. [[CrossRef](#)]
31. Mitchell, P.W. Climate Change Effects on Expansive Soil Movements. In Proceedings of the 18th International Conference on Soil Mechanics and Geotechnical Engineering, Paris, France, 2–6 September 2013.
32. Sun, X.; Li, J.; Zhou, A. Assessment of the impact of climate change on expansive soil movements and site classification. *Aust. Geomech.* **2017**, *52*, 39–50.
33. Karunarathne, A.M.A.N.; Gad, E.F.; Disfani, M.M.; Sivanerupam, S.; Wilson, J.L. Review of calculation procedures of Thornthwaite Moisture Index and its impact on footing design. *Aust. Geomech. J.* **2016**, *51*, 85–95.
34. Leao, S.Z. Mapping potential risk for housing damage from ground movement due to climate change. *Int. J. Environ. Sci. Dev.* **2014**, *5*, 387–392. [[CrossRef](#)]
35. Yue, E.; Chen, L.; Bulut, R.; Cheng, Q. Climatic Parameter TMI in Subgrade Soils. In *Climatic Effects on Pavement and Geotechnical Infrastructure*; ASCE Library: Reston, WV, USA, 2014; pp. 109–116.
36. Thornthwaite, C.W. An approach toward a rational classification of climate. *Geogr. Rev.* **1948**, *38*, 55–94. [[CrossRef](#)]
37. Thornthwaite, C.W.; Mather, J.R. The water balance: Centerton, N. J. *Publ. Climatol.* **1955**, *8*, 1–104.
38. Witzczak, M.W.; Zapata, C.E.; Houston, W.N. *Models Incorporated into the Current Enhanced Integrated Climatic Model for Version 1.0 of the ME-PDG*; Arizona State University: Tempe, AZ, USA 2006.
39. Amakye, S.Y.; Abbey, S.J. Understanding the performance of expansive subgrade materials treated with non-traditional stabilisers: A review. *Clean. Eng. Technol.* **2021**, *4*, 100159. [[CrossRef](#)]
40. Gudipudi, P.P.; Underwood, B.S.; Zalgout, A. Impact of climate change on pavement structural performance in the United States. *Transp. Res. Part D: Transp. Environ.* **2017**, *57*, 172–184. [[CrossRef](#)]
41. Ahmed, A. Effects of Climatic Loading in Flexible Pavement Subgrades in Texas. Ph.D. Thesis, University of Texas Arlington, Arlington, TX, USA, 2017.
42. AS2870. Residential slabs and footings. In *Standards Australia*; Standards Australia: Sydney, Australia, 2011.
43. Cameron, D.A. Dealing with reactive clay soils through a national standard. *Aust. Geomech.* **2018**, *53*, 51–65.
44. Hall, C.E.; Jones, S.A.; Bodorkos, S. Sedimentology, structure and SHRIMP zircon provenance of the Woodline Formation, Western Australia: Implications for the tectonic setting of the West Australian Craton during the Paleoproterozoic. *Precambrian Res.* **2008**, *162*, 577–598. [[CrossRef](#)]
45. Kaufmann, R.K.; Kauppi, H.; Mann, M.L.; Stock, J.H. Reconciling anthropogenic climate change with observed temperature 1998–2008. *Proc. Natl. Acad. Sci.* **2011**, *108*, 11790–11793. [[CrossRef](#)]
46. Mather, J.R. *Climatology: Fundamentals and Applications*; McGraw-Hill: New York, NY, USA, 1974.
47. Thornthwaite, C.W. The climates of North America: According to a new classification. *Geogr. Rev.* **1931**, *21*, 633–655. [[CrossRef](#)]

48. Thornthwaite, C.W.; Mather, J.R. *Instructions and Tables for Computing Potential Evapotranspiration and the Water Balance*; Laboratory of Climatology: Centerton, AR, USA, 1957.
49. Aitchison, G.; Richards, B. *Broad-Scale Study of Moisture Conditions in Pavement Subgrades throughout Australia*; CSIRO: Sydney, Australia, 1965.
50. Perera, Y.Y.; Zapata, C.E.; Houston, W.N.; Houston, S.L. Long-term moisture conditions under highway pavements. In *Geotechnical Engineering for Transportation Projects*; ASCE Library: Reston, WV, USA, 2004; pp. 1132–1143.
51. Rahman, M.M.; Beecham, S.; Iqbal, A.; Karim, R.; Rabbi, A.T.Z. Sustainability Assessment of Using Recycled Aggregates in Concrete Block Pavements. *Sustainability* **2020**, *12*, 4313. [[CrossRef](#)]
52. Smith, R. Estimating soil movements in new areas. In *Seminar-Extending the Code Beyond Residential Slabs and Footings*; The Institution of Engineers: Barton, Australia, 1993.
53. Olaiz, A.H.; Singhar, S.H.; Vann, J.D.; Houston, S.L. Comparison and applications of the Thornthwaite moisture index using GIS. In *Proceedings of the PanAm Unsaturated Soils*, Dallas, TX, USA, 12–15 November 2017; pp. 280–289.
54. McKeen, R.G.; Johnson, L.D. Climate-controlled soil design parameters for mat foundations. *J. Geotech. Eng.* **1990**, *116*, 1073–1094. [[CrossRef](#)]
55. Van Vuuren, D.P.; Edmonds, J.; Kainuma, M.; Riahi, K.; Thomson, A.; Hibbard, K.; Hurtt, G.C.; Kram, T.; Krey, V.; Lamarque, J.-F.; et al. The representative concentration pathways: An overview. *Clim. Chang.* **2011**, *109*, 5. [[CrossRef](#)]
56. TMK. *TMK Soil Movement Map*. 2021 [cited 2021 19/08/2021]. Available online: <http://www.tmkmaps.com.au/SoilMovement/> (accessed on 19 August 2021).
57. FMG; Ward, J.; Walsh, P.; Cameron, D. *Code Oriented Raft Design (CORD)*; FMG Engineering: Kent Town, SA, Australia, 2012.
58. Walsh, P.F.; Walsh, S.F. *Structure-Reactive Clay Model for a Microcomputer*; CSIRO Division of Building Research Report; CSIRO Division of Building Research: Melbourne, Australia, 1987.
59. Walsh, P.F. *The Analysis of Stiffened Raft on Expansive Clays*; CSIRO Division of Building Research Report; CSIRO Division of Building Research: Melbourne, Australia, 1978; p. 14.